P. Brisebois, M. Aouinti, M. Jafari,
M. Siaj,
C. Ouellet-Plamondon* 2400753

Adsorption Dynamics of Disodium Octaborate Tetrahydrate on Clay Minerals: Implications for Construction Wood Protection

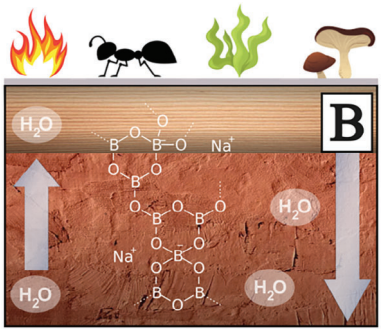

Clay has the adsorption capabilities to accelerate the leaching of wood preservatives. This is problematic for wood decay and fire protection in earthen constructions. Atomic force microscopy (AFM) and chemical mapping using photoinduced force microscopy (PiFM) of wood show that protective wood treatment is not uniform on the surface. Boron analysis is performed using inductively coupled plasma optical emission spectroscopy (ICP-OES).

small methods
www.small-methods.com

Adsorption Dynamics of Disodium Octaborate Tetrahydrate on Clay Minerals: Implications for Construction Wood Protection

*Patrick Brisebois, Meriam Aouinti, Maziar Jafari, Mohamed Siaj, and Claudiane Ouellet-Plamondon**

The wood preservative disodium octaborate tetrahydrate (DOT) migration is studied in clay. Using boron analysis by inductively coupled plasma optical emission spectroscopy (ICP-OES), DOT spatial and temporal dynamics are surveyed to show how DOT permeates into the wood and the clay using concentration profiles as a function of depth, initial wood moisture, and direction of filling. Atomic force microscopy and chemical imaging using photoinduced force microscopy are used to show the morphology of the wood samples and the distribution of DOT on their surface. ICP-OES results show that the average DOT concentration in the wood samples is originally 0.8 and 1.5 wt% in the bulk and at the surface, respectively. Conditioning of the wood to a moisture content of 19% in a climatic chamber reduces DOT concentration by 8% for the fir and 17% for the spruce. After one week of contact with the clays, the results showed a rapid decrease of 25–40% in DOT concentration in wood. On longer periods (5 months), the spruce shows a tendency to reabsorb the DOT from the clay and the DOT migration stabilizes at 20%. These results contribute to defining the dosage of DOT when the wood is exposed to clay.

1. Introduction

Wood is a renewable material and shows great potential in urban construction as a high-performance structural material[1–3] and in transparent composites for windows.[4] Natural wood structures require high physical, biological, and mechanical properties to sustain the construction of buildings and to retain their architectural integrity over their lifespan.[5] A common practice to protect natural wood from decay caused by fire, insects, algae, and fungal attacks is to coat lumber with chemical preservatives to provide superior performance.[6] In the United States, the most widely used building code is the International Building Code, which requires that wood used for building framing and perimeter walls be treated for fire protection (Type III).[7] Frequently employed chemicals for wood preservatives are tars and oils, organic fungicides (chlorinated, azoles, and carbamates), silicates, copper salts, and boric acid salts (borates).[8–11] Borates have been increasingly used in the preservation industry because they are effective in preventing wood decay,[9] and have noticeable flame-retardant properties.[12,13] Noteworthy, borates are eco-friendly[14,15] and show a low impact on drinking water and human health.[16] On a large scale, they are easily applied to wood by wetting and dipping techniques.[17] Diffusion of small molecules including borate and water through the cell wall structure of wood[18,19] is governed by nanoscale ion transport and regulation dynamics.[20] Due to their naturally high mobility in wood, borates are problematic for protecting exterior wood because they can leach out and be in contact with rainwater, soil, and other materials.[21] Water-soluble preservatives, by nature, are prone to leaching when exposed to moisture. This leads to a gradual loss of the preservative from the wood, reducing its effectiveness over time. This limits borate to interior and framing applications in situations where the treated wood product is not being directly exposed to water, and where an exterior plaster or other building envelope components are added. In earthen constructions, one of the world's oldest and most ecological construction methods,[22] the woodwork is often in contact with natural grains such as clay outsourced locally.[23] As the industry moves toward more sustainable practices, it is imperative to explore alternative preservative technologies that offer enhanced performance and environmental safety. Disodium octaborate tetrahydrate (DOT), a soluble borate salt prepared at the industrial scale, has not yet been used to treat wood in combination with clay and requires validation prior to being used in earthen

P. Brisebois, M. Aouinti, C. Ouellet-Plamondon
Department of Construction Engineering
École de technologie supérieure, Université du Québec
1100 Notre-Dame St. W., Montreal, QC H3C 1K3, Canada
E-mail: Claudiane.Ouellet-Plamondon@etsmtl.ca
M. Jafari, M. Siaj
Department of Chemistry
Biology
Université du Québec à Montréal
2101, Montreal, QC H2X 2J6, Canada

The ORCID identification number(s) for the author(s) of this article can be found under https://doi.org/10.1002/smtd.202400753

DOI: 10.1002/smtd.202400753

constructions. Wood and bio-based materials commonly used in earthen construction are promising to lower the carbon impact of construction, in regions where cement is not produced and where housing is needed.[24,25]

Clays are used in construction in the form of bricks, blocks, roof tiles, pavers, ceiling plaster, and finishing plaster.[26,27] Clay minerals are composed of silicon, aluminum, oxygen atoms, and exchangeable cations like sodium (Na^+), magnesium (Mg^{2+}), and potassium (K^+) assembled into single layers, particles, and aggregates of particles.[28] Clays are porous, thermally insulating,[29] and have adsorptive and ion-exchange properties.[30] There are two types of adsorption in clays: physical adsorption and chemical adsorption. Physisorption is a type of weak and reversible adsorption involving Van der Waals and capillary forces that hold molecules in multilayers on a surface. For chemisorption, the molecules interact chemically with the surface resulting in the formation of strong and irreversible covalent bonds between the adsorbent (borates) and the adsorbate (clay).[28] This is problematic because the adsorption of the chemical preservatives by the clay in contact with woodwork changes the physico-chemical properties of the clay[31] and accelerates leaching, thus exposing the wood to less protection against decay.

The identification of the change in the chemical composition of wood can be achieved by using analytical techniques that allow the qualitative as well as quantitative determination of the chemical constituents present in the wood samples.[32] These techniques include vibrationalspectroscopy, mass spectrometry, X-ray diffraction, scanning and transmission electron microscopy, and solid-state nuclear magnetic resonance.[32,33] One convenient way for analyzing boron (B) in materials accurately is inductively coupled plasma (ICP) spectrophotometry in solutions on samples digested in hot acid or base.[33] ICP is the most sensitive method currently available. ICP is routinely used in multi-element analysis of clays[34] and for boron analysis of treated solid wood.[35]

For materials applications, it is critical to understand and control the transport of ions such as borates in wood[20] and how this might affect the surrounding material properties for construction purposes.[7] A better understanding of these aspects will accelerate the development of greener and more durable woodworking products, expanding the market of sustainable earthen constructions.[8] In this context, we studied the migration of DOT from treated fir and spruce (supplied by Boralife Technologies Inc.) into clay mixtures (red and beige). DOT has the elemental formula $Na_2B_8O_{13}$-$4H_2O$ and is used commercially as a wood preservative.[8,11] To accomplish this, DOT concentration in the materials was evaluated in terms of boron analysis. Boron analysis was carried out on acid digested fractions by inductively coupled plasma optical emission spectroscopy (ICP-OES) of both the clay and the wood.[36] DOT migration and concentration profiles are used as a function of depth, contact time, initial wood moisture, and direction of filling (vertical↑, lateral→ and gravitational↓). Herein, using atomic and photoinduced force microscopy (AFM-PiFM) chemical mapping, we show how DOT is distributed on the surface of the treated wood samples. Also, using zeta potential values, we show how the colloidal properties of the clay are affected by the adsorption of DOT.

Table 1. Chemical composition of the clays.

Element	Red Clay [at%]	Beige Clay [at%]
Oxygen (O)	48.8 ± 0.4	49.6 ± 0.5
Silicon (Si)	31 ± 1	32 ± 1
Aluminium (Al)	10 ± 2	12 ± 1
Iron (Fe)	5.4 ± 0.2	1.6 ± 0.4
Potassium (K)	2.7 ± 0.1	2.8 ± 0.2
Magnesium (Mg)	0.6 ± 0.1	0.6 ± 0.1
Titanium (Ti)	0.4 ± 0.2	0.5 ± 0.2
Barium (Ba)	0.5 ± 0.3	0.4 ± 0.2
Calcium (Ca)	0.3 ± 0.1	0.1 ± 0.1
Phosphorus (P)	0.1 ± 0.1	ND

ND = non-detectable

2. Results and Discussion

2.1. Characterization of the Clay

The characterization aimed to elucidate various physical, chemical, and mineralogical properties of the clays, providing valuable insights into their geotechnical properties and their potential applications in construction.[27] First, the particle size analysis revealed that the clay samples predominantly consist of fine particles. For both types of clays (Midstone: beige clay and Redstone: red clay), the particle size varies mainly between 0.40 and 250 µm, with the most abundant density around average particle size of 15.0 to 20.0 µm. The standard deviation (SD) with laser granulometry was ≈2%. X-ray diffraction (XRD) analysis showed prominent peaks corresponding to elements such as oxygen, silicon, aluminum, iron, potassium, magnesium, titanium, barium, calcium, and phosphorus (**Table 1**).

XRD spectrum (**Figure 1**) also showed that quartz is the dominant constituent in both clays. Other minerals that contribute significantly to the composition of the clays are illite, muscovite, and kaolinite, while hematite was detected in smaller amounts

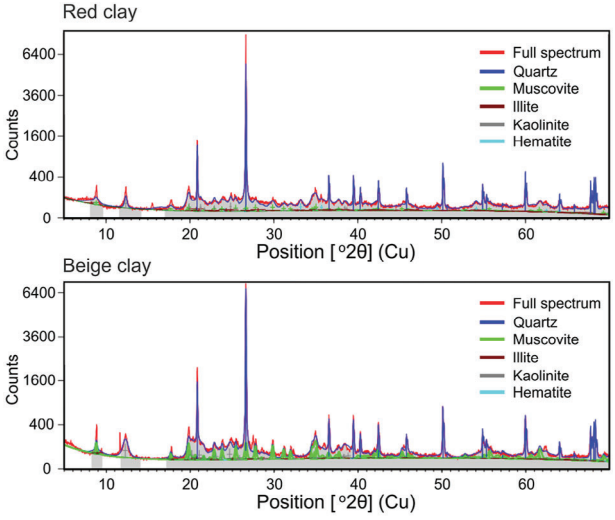

Figure 1. XRD spectra (full spectrum) of the red and beige clays.

Table 2. Mineral composition of the clays.

Mineral	Red Clay [wt%]	Beige Clay [wt%]
Quartz	42.4 ± 0.5	42.5 ± 0.5
Muscovite	24 ± 3	17.5 ± 0.7
Illite	22 ± 1	14.2 ± 0.8
Kaolinite	9.3 ± 0.4	25.7 ± 0.7
Hematite	2.2 ± 0.2	0.2 ± 0.1

(**Table 2**).[37] Noteworthy, these minerals have low absorption capacity compared with other clay minerals (montmorillonites, smectites, etc.).[31] Based on their mineralogical composition, it is therefore suggested that both clay types have limited sorption capabilities toward the DOT preservatives contained in the wood. Furthermore, XRD results also showed that the red clay contains 2.2 wt% of hematite which explains its color.[38]

Atterberg limits were calculated to identify and describe the plasticity domain of the two types of clay by means of the plasticity indices (PI), which indicate if clay possesses significant plasticity and moldability when moistened in terms of compressibility and permeability.[39] This is an important feature in construction, to avoid any risk of structure instability and build with long-lasting structural durability.[40] According to our experiments, the liquidity limit (LL) was between 32 and 34% for the clays. The plasticity limits (PL) were between 15 and 16%. These (LL and PL) values are typical of several earth materials such as compressed earth blocks and adobe bricks that have plasticity limits between 15 and 29%.[41] PI was calculated from the difference between the liquidity and the plasticity limits (PI = LL – PL). PI values were between 17% and 18%. Based on the Casagrande diagram, this plasticity belongs to the category of moderately plastic clays (10% <PI> 35%).[42] Clays with plasticity indices less than, or equal to, 18% also have a low swelling potential.[43] The latter is a key parameter in the selection of building materials and is important for assessing the suitability of clays for construction purposes[44] and for avoiding geotechnical problems associated with swelling clays.[45]

2.2. Characterization of the Wood

The chemical composition of the solid wood surface was analyzed using attenuated total reflectance infrared spectroscopy (ATR-IR) and photoinduced force microscopy (PiFM), while morphology was evaluated using optical and atomic force microscopy (AFM). ATR-IR is a useful method to study wood and spectra (**Figure 2**) acquired on the samples were compared with reference spectra of known wood components to validate the identification of functional groups.[33,46,47] Subtle variations in the intensity of certain peaks were observed, suggesting differences in chemical composition between the fir and the spruce species. Both wood samples showed a strong, broad peak ≈3400 cm^{-1}, indicating the presence of cellulosic hydroxyl groups (OH). Peaks at ≈2900 and 1370 cm^{-1} were attributed to stretching vibrations of C-H bonds (cellulose). For hemicellulose, two strong peaks at 1050 and 1090 cm^{-1} and a broad signal at 1600 cm^{-1} indicated the presence of C—O stretching, and carboxylate (COO^-) stretching, respectively. The presence of lignin was indicated by peaks at ≈1500 cm^{-1} (aromatic backbone vibrations) and 1250 cm^{-1} (C—O—C stretching).[48]

2.3. Characterization of the DOT Treated Wood

By comparing ATR-IR spectra of DOT treated and untreated (fir and spruce) wood samples, we were not able to highlight the presence of borates with certainty (not shown). This is because the signals of borates overlap with the signals of cellulose, hemicellulose, and lignin of the wood in the ATR-IR analysis (Figure 1).[49] To help us identify the changes associated with the presence of borates, spiking the samples with boric acid was performed. To do so, the untreated wood samples were cut into 1 cm × 1 cm × 1 cm cubes, then immersed in 0 (pure

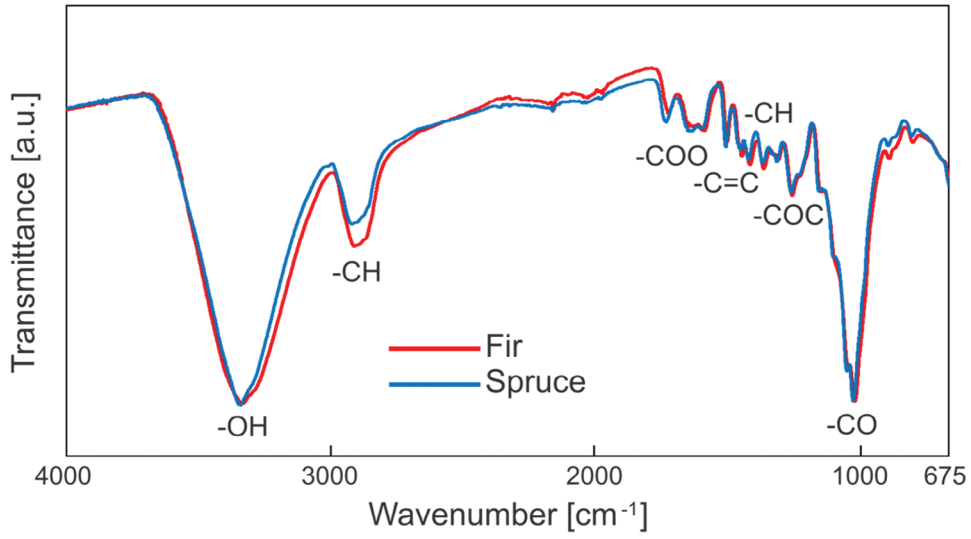

Figure 2. ATR-IR spectra (full spectrum) of the untreated fir (red) and of the untreated spruce (blue) wood samples.

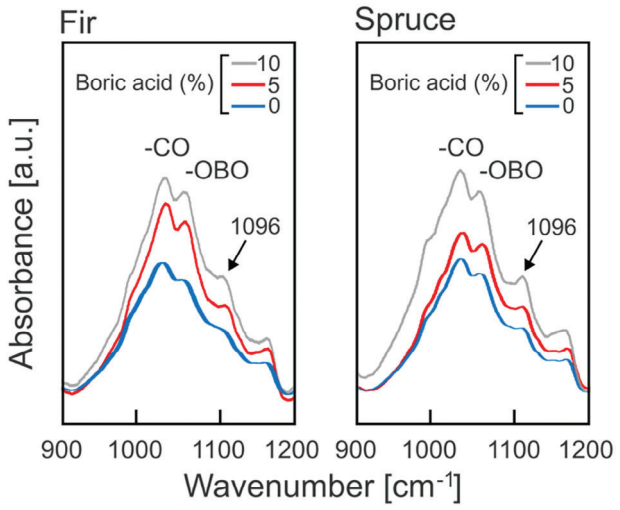

Figure 3. ATR-IR spectra of the fir and of the spruce wood samples spiked with 5% and 10% boric acid solutions.

water), 5 or 10% (w v^{-1}) reagent grade boric acid solutions for 24 h. The cubes were dehydrated in an oven at 40 °C for 3 days prior to analysis. Even after spiking the wood samples, ATR-IR could not detect new distinct peaks corresponding to different functional groups present in borates.[49] Based on the observed shifts, intensities, and changes in peak shapes in the signals of the wood spectra, it was inferred that certain chemical changes occurred in the wood samples after the spiking. A series of intensity changes in peak between 1100 to 1475 cm^{-1} for both wood species was observed, which is characteristic of the two bands of boric acid at 1150 and 1429 cm^{-1}.[49] **Figure 3** shows the region that was the most sensitive to the spiking experiments of both wood species, with the most noticeable peak intensity change at 1096 cm^{-1}.

Prior to performing PiFM surface chemical mapping, the topographical features of the wood substrates were examined using a tapping mode AFM (**Figure 4**). The images exhibited a highly complex and hierarchical structure, which is characteristic of natural wood, including features like grain patterns. Darker regions represent wood cracks and pits in the AFM images, while lighter regions are representative of higher grain.[50] PiFM is a powerful technique that combines AFM with IR-absorption spectroscopy, enabling the simultaneous acquisition of high-resolution topographical information and chemical vibrational spectra with nanoscale spatial resolution.[51,52] By measuring the IR wavelength-specific induced change in surface molecules' dipole moments at each pixel of the AFM scan, a chemical map is generated by highlighting different chemical components present in the wood. Figure S2 (Supporting Information) shows the IR spectra acquired by the PiFM technique. Observed signals include cellulose, lignin, hemicellulose, and additives (DOT) as described by ATR-IR. Figure 4 shows the PiFM intensity image with the spatial distribution of DOT across the sample. The chemical mapping images were plotted at 1096 cm^{-1} to cover the signal increase after DOT treatment and to make the PiFM image more sensitive and representative of the treatment effects. The chemical mapping revealed that DOT distribution is not uniform across the wood surface. Instead, DOT tends to accumulate in island-like regions. The brighter regions correspond to areas of higher DOT concentration. By comparing the AFM and PiFM images, the DOT treatment has accumulated mainly on the surface of the wood, with less penetration into the cracks and pits (Figure 4). Furthermore, optical magnification at 500× using a Kenyence (VHX7000) microscope revealed distinct crystalline structures (sap) that supported the smooth surface and wood fibers (Figure 4). Light microscopy also revealed the presence of defects and anomalies within the wood grain. These included cracks and irregularities in the fiber orientation. Wood's surface structure and integrity are important considerations when defining preservative dynamics. The porosity of the wood and the degree to which the pits are closed or aspirated will affect both the treatability of the wood and the retention of the DOT.[53]

2.4. Adsorption Tests

To study the DOT migration phenomenon, three tests were conducted to see how DOT leached from the wood and was adsorbed on the clays: 1) tests by migration direction, 2) tests by wood moisture content, and 3) tests by contact time. The formulation of the clay pastes consists in mixing a quantity of red or beige clay with water, with a water/clay ratio equal to 0.25, in order to obtain realistic pastes representative of the samples to be used directly for the construction of wooden frames.[37] Before proceeding with the contact between the wood and the clay, the wood samples (width ≈3 cm; thickness ≈4 cm; length ≈9 cm) were cut from the whole panel and placed at the bottom of a non-absorbent plastic form. A thick layer (≈5 cm) of clay paste (≈370 g) was then applied by hand to the top of the wooden sample (≈35–38 g) to cover the entire upper part of the mold. The assembly was covered and kept horizontally (vertical migration) or rotated 90° (lateral migration) and 180° (gravitational migration) in an airtight bag to prevent moisture loss by evaporation and stored at room temperature (22 C°) for a variable period (1 day to 5 months). At the end of the migration experiment, the form was disassembled, and the bulk layers were separated. Each layer (wood and clay) was cut in 4 equal fractions of equal thickness (≈1 cm) using a band and wire saw (Figure S1, Supporting Information), respectively, and labeled 1 to 8. Each fraction was then dried, pulverized, digested, and analyzed for boron concentration using ICP-OES (see section 4.8). The DOT determination was made by subtracting the amount of boron naturally present in the materials. For the effect of moisture, two types of wood were used, the first was unconditioned, that is, as received from the manufacturer with a low moisture content of (9.0 ± 0.1) % (determined upon receipt), and the second was conditioned to a medium moisture content of (19.0 ± 0.1) %,[54] which represents the maximum moisture level allowed by the International Building Code.[7]

2.5. Changes in DOT Concentrations with Migration Direction

In construction, wood-clay interfaces may be oriented horizontally or vertically. Questions were raised if the orientation of the clay relative to gravity influenced DOT migration in unconditioned wood lumbers. Results show the DOT migration (%) in

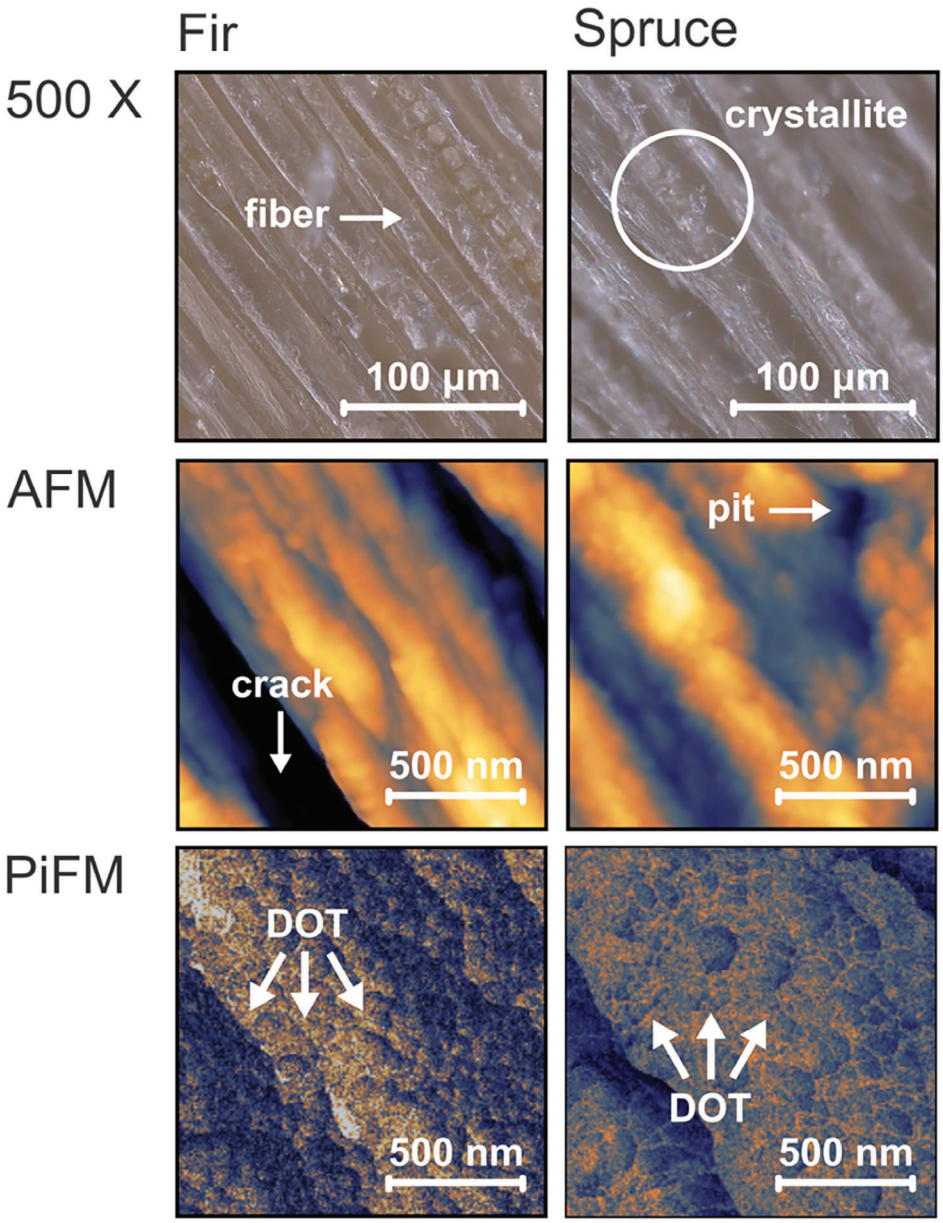

Figure 4. Optical images (500 ×), AFM, and PiFM mapping of the surface of the fir and the spruce wood samples treated with DOT.

the fir and the spruce samples after contact with the red and the beige clay for one week. Percentages were calculated relative to the total amount of DOT initially present in the wood samples. The average DOT concentration in the bulk of the wood samples were initially (0.89 ± 0.04) and (0.82 ± 0.06) wt% for the unconditioned and conditioned fir respectively, and of (0.81 ± 0.02) and (0.67 ± 0.05) wt% for the unconditioned and conditioned spruce. The conditioning of the wood lowered the DOT concentration by ≈8% for the fir, and 17% for the spruce. DOT migration was found to be 22–40% after sorption by the clays. Higher losses of (40 ± 5) % were obtained for the fir in contact with red clay in the lateral alignment, while the fir in contact with beige clay showed the smallest decrease of (22 ± 4) % in the gravitational direction. The results show averaged DOT migration of (37 ± 3) %, (36 ± 4) %, and (30 ± 8) % for the vertical, lateral, and gravitational orientations, respectively. A single-factor ANOVA test of comparison was used to analyze the data among the three orientations. The P-value was estimated to 0.2 with $\alpha = 0.05$, n = 4, and k = 3 (Table S1, Supporting Information). Consequently, the filling direction did not significantly affect DOT diffusion through the fir and spruce in our experiments.

2.6. Changes in DOT Concentrations with Humidity

Diffusion of DOT and water in wood occurs in a broad spectrum of moisture content (MC), and diffusion rates are expected to rise with increased MC. However, diffusion becomes a complicated

Table 3. Effect of wood moisture on the leaching of DOT in treated wood after one week of lateral contact with the clay.

		DOT migration [%]			
		Day 1		Day 7	
Wood	Clay	9%	19%	9%	19%
Fir	Red	32 ± 2	34 ± 1	40 ± 5	39 ± 1
Fir	Beige	27 ± 6	24 ± 5	31 ± 6	30 ± 5
Spruce	Red	29 ± 2	22 ± 5	37 ± 3	27 ± 5
Spruce	Beige	32 ± 2	23 ± 8	35 ± 2	25 ± 4

process when water does not uniformly permeate the samples.[18] **Table 3** shows how the DOT migration in the wood samples (fir and spruce) is affected by humidity over a one-week period of contact with the clay in the lateral orientation.

At day 1, DOT migration was found to be between 22 and 34%, with conditioned spruce at 19% moisture content showing the smallest decrease of 22–23%. After one week, the loss slightly increased (25–40%) for both unconditioned (9%) and conditioned (19%) wood. Higher values up to 40% were then obtained for the fir in contact with the red clay. A *t*-test of comparison of the mean ($n = 4$, $k = 2$, $\alpha = 0.05$, $P = 0.01$) was used to show that increasing time contact from 1 day to 1 week has a significant effect on the increase of DOT migration for the unconditioned wood (Table S2, Supporting Information). In the same trend, a *t*-test ($n = 4$, $k = 2$, $\alpha = 0.05$, $P = 0.003$) showed that the red clay is likely to increase DOT migration by 20% for the fir compared to the beige clay (Table S3, Supporting Information) in the moisture condition studied (9% and 19%). This may be related to the changing strength of retention of DOT with the extractive clay materials.[30]

2.7. Spatial Changes in DOT Concentrations

Water movement in wood is the driving force for DOT migration. It occurs by several pathways, including water vapor diffusion, cell wall water diffusion, and capillary water transport. Diffusion is the net flow of mass resulting from random molecular motions. Water is present both in the cell walls and in the porous structure of the material. The absorption of water in the cell wall involves several physicochemical phenomena that can affect the equilibrium position.[52] Consequently, the dynamic state of DOT within the wood cells results in a continuous migration of the mobile components in the clay direction within the wood. This results in a redistribution of DOT within the wood as well as migration into the clay environment outside the wood. DOT diffusion is predictable in wood saturated with water: it will follow differences in concentration among its path to the clay.[53]

Experimentally, the eight fractions obtained from the wood and clay cutting (Figure S1, Supporting Information) were regrouped into statistical groups ($k = 8$) and their averages were analyzed individually. The value of DOT concentration corresponding to each fraction was calculated from the average of the results ($n = 24$) obtained from the four (4) types of wood combination (unconditioned, conditioned, fir, and spruce) in contact with the two (2) types of clays at the three (3) different stages (day, 0, day 1, and day 7). A single factor ANOVA test ($\alpha = 0.05$) showed a very high variance between the data collected and a low P-value (1×10^{-85}), indicating that the averaged DOT concentration in each fraction was statistically different and can be compared. Within each fraction, further ANOVA tests for the effect of time also showed a significant change in DOT concentration between the different days ($P = 0.04$ to 0.00001), except for fraction 3, where DOT concentration remained the same statistically over the week period ($n = 8$, $k = 23$, $\alpha = 0.05$, $P = 0.4$) (Table S4, Supporting Information). **Figure 5** shows the concentration profile of DOT (wt%) in the different fractions (1–8) changing over one week of migration in the lateral position. Each wood fraction was ≈1 cm thick, while each clay fraction was ≈1.25 cm thick.

The results show that the initial depth distribution of DOT in wood is not uniform; the majority of DOT is concentrated on the surfaces of the wood sample. The initial DOT concentrations were (1.5 ± 0.3) and (1.1 ± 0.1) wt% for layers 1 and 4, respectively, which represent a difference of almost 28% between the mass concentrations on the two sides. The heterogeneity of DOT treated wood as well as the DOT concentration standard deviations led to measurements with uncertainties in the results. These variations in the initial DOT concentration were explained by the impregnation profile, which varies from one board to another due to different parameters: wood species, age of impregnation, DOT retention rates, and origin of the board (tree, position in the tree). In our experiments, all assemblies were oriented with the DOT-rich part of the wood away from the clay. After migration, the decrease in DOT concentration was on average greater in layer 4. After a contact time of 24 h, the amount of DOT adsorbed in the clay was concentrated at the disk in direct contact with the wood (layer 5), reaching a maximum concentration of (0.11 ± 0.04) wt%. When the contact time was extended to one week, a decreasing migration profile was observed from layer 5 to the surface disks (6, 7 then 8). The DOT concentration in the clay (layers 5–8) increased with increasing contact time, going from 0 to 0.06 wt%. The DOT in the clay layers is more diluted than in the wood because ≈10 times more clay (370 g) than wood (35-38 g) is used for the sorption test.

2.8. Long-Term Changes in DOT Concentrations

After being aged in contact with the clay under specific humidity and temperature conditions, the wood sample ultimately dries. As wood dries, its internal condition alters gradually. Consequently, there will be unsteady flow, and the diffusion coefficient of DOT will fluctuate. Thus, the distribution of moisture within the wood, and how it shifts over time, are crucial factors for forecasting how DOT behaves in the wood samples.[18,55,56]

For a longer period of contact, **Figure 6** shows the concentration of DOT in unconditioned (MC = 9%) spruce up to 5 months of lateral contact with the red clay. Values are compared to the control experiment (0.80 wt%) when the spruce is in contact with no clay in the form for 5 months. The standard deviation in the control (SD = 0.02 wt%) is mainly caused by the variability in the wood treatment. Looking at the evolution: two phases occurred. The results show a quick decrease in DOT concentration in spruce for the first week phase going from (0.81 ± 0.02) wt% to ≈(0.51 ± 0.03) wt%. After which this amount tends to increase slowly up to (0.70 ± 0.05) wt% at month four and then stabilizes

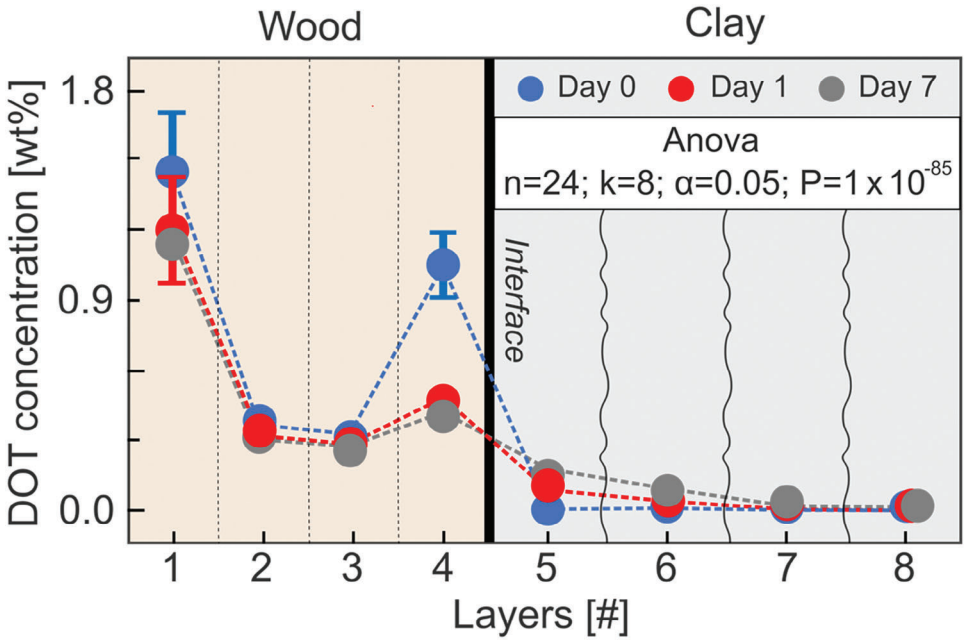

Figure 5. Effect of time on the concentration profile of DOT in wood and clay (lateral migration).

≈(0.65 ± 0.06) wt% in the final phase of the 5-month period. Statistical analysis using the ANOVA test on the data set presented in Figure 6 showed that the change in DOT concentration over the 5-month period was significant (n = 3; k = 8, α = 0.05, P = 0.0007). Further *t*-tests on every pair of data confirmed that differences were all significant when compared to the control experiment and the initial state (n = 3; k = 2, α = 0.05, P = 0.001 to 0.047).

In the first week, the quick drop in DOT concentration shows that borates escaping from the wood is a fast process. DOT leaching is important at early stages because the wood is still humid, and the DOT is carried by water. After the first month, samples showed obvious signs of wood drying, such as cracking in the mold and shrinkage due to moisture loss, which slowed down DOT mobility. Wood is a porous and hygroscopic material.[56] Two months into the process, the wood begins to reabsorb water vapor from the clay, leading to an increase in its weight. This continues until the wood's moisture content balances with the relative humidity (RH) and temperature of the clay. The sorption process is characterized by the forming and breaking of strong intermolecular bonds among water molecules, the wood preservative (DOT), and wood polymers. During this process,

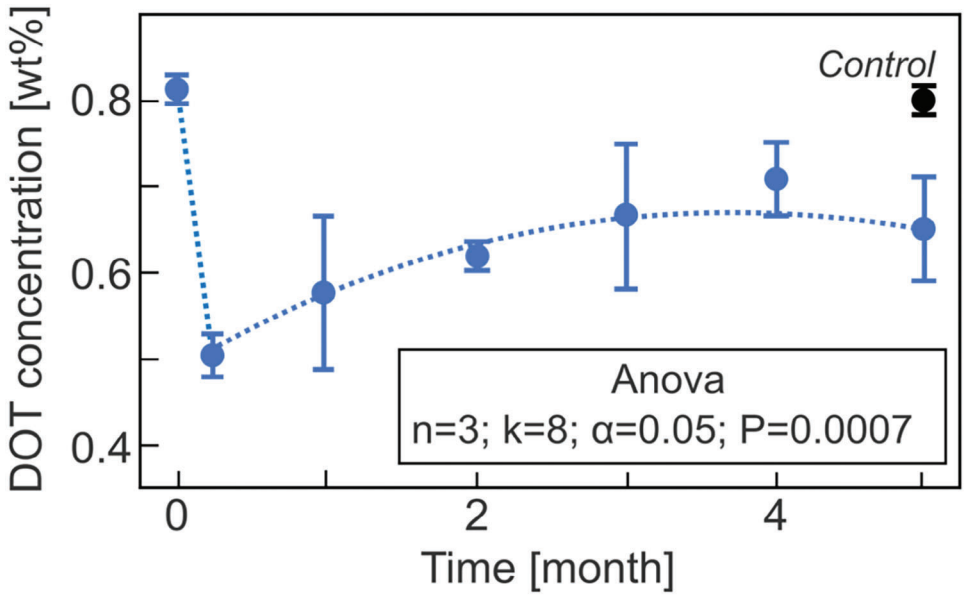

Figure 6. Effect of time on the concentration of DOT in spruce (lateral migration) with a moisture content of 9% in contact with the red clay.

water molecules move in two ways: absorption, where the wood takes in water vapor, and desorption, where it releases water vapor back into the clay.[55] After a period of 5 months, the wood stabilizes at an equilibrium state where its weight remains constant, provided that environmental conditions do not change. The adsorption of water happens through the sorption of water vapor. This process involves water molecules transitioning from a vapor state in the sample to a condensed state within the wood, either within its cell walls or its capillary structures.[55] Overall, the experiments showed that the unconditioned spruce lost ≈(20 ± 2) % of its protective treatment over 5 months of contact with the red clay.

2.9. Changes in the Colloidal Properties of Clays

Clay mineral adsorption of ions and molecules impacts their hydration and swelling and also alters their porosity and coats their surfaces. Additionally, the surface tension at the interface between clay minerals and water is modified because of the influence of the ions on the physico-chemical properties (dielectric constant, refractive index, and viscosity) of water.[57] Zeta potential significantly informs the properties and behaviors of clays, particularly in water-based environments. It refers to the electrostatic charge on clay particle surfaces when dispersed in a liquid, typically water, and affects how these particles attract or repel each other. The Derjaguin-Landau-Verwey-Overbeek (DLVO) theory posits that the colloidal stability of particles like clay is dictated by the interplay between these repulsive and attractive forces.[58] This interaction can affect clay flocculation and its usability in construction. Numerous studies have explored how pH changes impact the zeta potential of clay minerals.[59] Literature also indicates that the sedimentation patterns of particles in colloidal systems are shaped by various factors, including specific interactions and the viscosity and ionic strength of the solution, which may lead to aggregation and decrease colloidal stability.[60] Thus, zeta potential is crucial for managing the dispersion, stability, rheological properties, and strength of clays in different cement-based applications.[61,62] According to the DLVO theory, the repulsive forces between particles stem from their surface charges, which is approximated by their zeta potential. In our study, we assessed the zeta potential of the clays both before and after adsorbing DOT. These clays were mixed in deionized water at a concentration of 1 g l^{-1} and agitated on a rotary shaker at 40 rpm for one week with and without 5 wt% DOT (50 mg). DOT concentration in the clay was ≈50 times higher than what was observed in the migration experiments described in Section 2.6. to exaggerate the effects that may be caused by excess exposure to DOT since insignificant changes (t-test: n = 6, k = 2, $\alpha = 0.05$, P = 0.3) were noted at lower concentration (e.g., 1wt%) for the beige clay. The pH levels of the solutions were checked using a pH meter before conducting the zeta potential measurements. Our findings indicate that borate ion adsorption slightly raised the pH levels in clay suspensions and the ANOVA test showed that the zeta potential was altered significantly (n = 6; k = 4, $\alpha = 0.05$, P = 0.0008). Both types of clay exhibited anionic properties. Following the absorption of DOT, the pH increased from 7.0 to 7.4, while the zeta potential shifted from (−11.6 ± 0.7) mV to (−17.6 ± 0.3) mV in red clay, and from (−17 ± 1) mV to (−22.8 ± 0.4) mV in beige clay

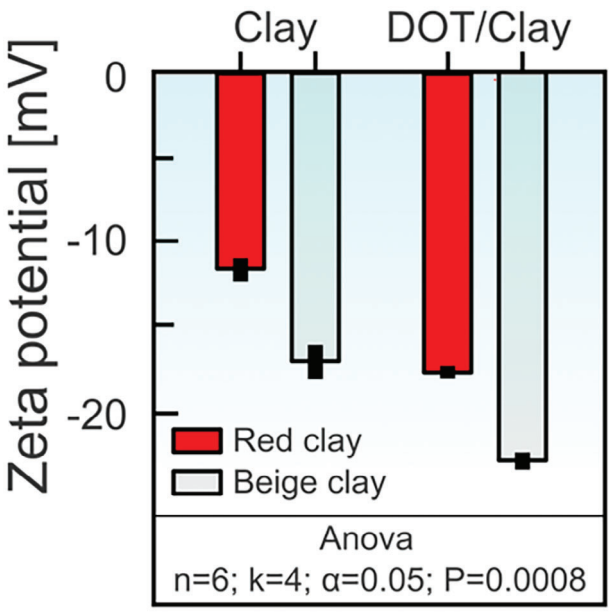

Figure 7. Zeta potential of the red and beige clays with and without 5 wt% of DOT.

(**Figure 7**). A rise in the absolute value of the zeta potential signifies an enhancement in surface charge. Accordingly, the data shows that the beige clay was more anionic and possessed superior colloidal attributes compared to the red clay.[57] Moreover, DOT's addition raised the absolute values of the zeta potential for both clays, suggesting an enhancement in their overall colloidal stability. These observations imply that DOT enhances the colloidal properties of clays, which points to improved long-term stability and workability.[59,60–62]

3. Conclusion

In summary, we have outlined a possible mechanism for the transfer of DOT preservatives from wood to clay minerals. This assessment of migration utilized the ICP-OES methodology. We employed relevant statistical analyses to show that factors such as moisture content, wood type, clay type, and the direction of migration relative to gravity had minimal or no significant statistical impact on the quantity of DOT that leached from the wood. Instead, the duration of contact with the clay was a more significant factor affecting DOT migration. Additionally, our depth analysis revealed an uneven distribution of DOT within the wood, primarily accumulating on the surface with a 28% variance noted between the two surfaces. At the interface, higher DOT concentrations were found in the clay directly in contact with the wood during sorption.

From a practical standpoint, the loss of water-soluble preservatives results in reduced protection against wood-degrading organisms. Comparatively, oil-based, fixed, or water-repellent preservatives offer more durable solutions, maintaining their protective qualities even under harsh environmental conditions.[63] This study shows that a 20% leaching of DOT can occur in clay minerals and this value stabilizes in time. Therefore, the wood treatment can be calibrated accordingly to keep the benefit of

DOT as an accessible wood treatment process for fire and insect protection. Furthermore, adsorption of DOT altered the zeta potential of the clay suspensions to more negative values, indicating that DOT does not cause flocculation of the clays over time, thereby not affecting their workability.

4. Experimental Section

Sample Preparation: Red (Redstone) and beige clays (Midstone) were from Plainsman (Alberta, Canada). For the experiments, powder clay was mixed manually with water to obtain a paste with a water-to-clay ratio of 25% with a density of (2.76 ± 0.05) g cm^{-3}. DOT-treated and untreated (virgin) wood boards of fir and spruce were provided by Boralife Technologies Inc. (Québec, Canada). Wood was impregnated with DOT (≈1–2% w w^{-1}) by soaking in hot concentrated DOT solutions.[17] The density of the unconditioned wood boards was 0.33 and 0.37 g cm^{-3} respectively for the fir and the spruce. Wood moisture conditioning was carried out according to the standard ASTM D4933 using a Thermotron climatic chamber.[50] Hydration of wood was performed at 22 °C and a relative humidity of 90%.

Laser Particle Sizing: Mean and size distribution of clay particles were measured using a Mastersizer 3000 (Malvern Pananalytical) laser diffraction particle granulometer equipped with a Hydro EV accessory, which was a dispersion unit for liquid channels equipped with a centrifugal pump, an immersion stirrer, and a 40 W ultrasonic probe for rapid particle dispersion. Clay powder (10 to 20 mg) was added directly into the semi-automatic mixing chamber containing deionized water (500 ml).

X-Ray Diffraction (XRD): XRD of clays was performed using a Bruker D8 Advance diffractometer operating at 40 kV and 40 mA with a copper (Cu) anticathode. The geometry used was of the Bragg-Brentano type. The XRD analysis was performed with an incident beam divergence of 0.26° (0.5 mm), and a 1.10° (2.5 mm) anti-reception scattering slit. Clay samples were rotated around the goniometer's vertical axis at 15 rpm to improve particle statistics, and measurements were taken over 5° to 70° 2θ with a step size of 0.020° 2θ. With a cumulative time per step of 0.50 s, the total measurement time was of 28 min per analysis. XRD analysis was performed on three different clay fractions: 0 – 20, 20 – 63, and 63 – 2 mm. These were prepared using the Sonic Sifter Separator model L3P ultrasonic sifter. XRD preparation began with grinding samples (5 g) with isopropanol (25 ml) using the XRD McCrone mill for 5 min at speed 3, followed by Buchner vacuum filtration with filter paper (N°50) and oven drying for 30 min at 40 °C.

Determination of Atterberg Limits: Liquidity and plasticity limits were measured using the Casagrande apparatus, according to the Canadian National Standard (CAN/BNQ 2501-090, C2011).[39] To measure the liquidity limit, ≈250 g of each type of clay was weighed, and a mass quantity of water between 20 and 30% was added.

Attenuated Total Reflectance Infrared Spectroscopy (ATR-IR): ATR-IR spectra were recorded on a Nicolet 4700 spectrophotometer (Thermo Scientific) equipped with a diffuse reflection attachment to optimize the collection of scattered radiation from a solid sample. The spectra were recorded with 64 scans in the spectral window between 675 and 4000 cm^{-1}. Atmospheric carbon dioxide (CO_2) and baseline corrections were automatically applied to the obtained spectra.

Atomic Force Microscopy (AFM): The AFM frames were taken on a Bruker Multimode8 Advanced microscope with a silicon nitride tip (2–12 nm nominal radius) in ScanAsyst-Air mode. The frames were determined by scanning a larger 20 μm^2 area and zooming in on a 2 μm^2 box where the flatter and more fiber-like locations of the surface were observed, to represent the longitudinal cut along the wood grain growth axis. The scans were resolved at 256 × 256 pixels and scanned at 1 line per s.

Photoinduced Force Microscopy (PiFM): PiFM was performed on VistaScope (Molecular Vista Inc, San Jose, CA, USA) which consists of an AFM aligned with a quantum cascade laser (QCL) source in the mid-infrared from 770 to 1910 cm^{-1} (Block Engineering, Southborough, MA, USA). The probe used was a gold-coated cantilever with a ≈20 nm radius of curvature tip (cleaned and sold by MolecularVista Inc.). The laser power was held at a baseline value of 7% and chemical mapping was traced at 1096 cm^{-1}, representative of the DOT functionalization. Images were treated with MolecularVista licensed software. Wood samples were glued to a 12 mm diameter magnetic sample port with instant glue to prevent sample movement during the analyses.

Inductively Coupled Plasma Optical Emission Spectroscopy (ICP-OES): ICP-OES analysis was performed on the Agilent 5110 spectrometer. The wood powder samples were digested according to the analytical method MA200-Met 1.2 (2020).[33] Briefly, the wood samples were dried at 104 °C for 24 h, ground into powder using an SM300 mill (1 min, 1000 rpm) and a coffee grinder (5 min), and sieved using 600 µm metal drum sieves. Then (2.000 ± 0.001) g of wood powder was mixed with 50% nitric acid (8 ml) and 20% hydrochloric acid (20 ml) for digestion. The acids-wood mixture was heated to reflux on a hot plate for 60 min without stirring, then cooled for 30 min at room temperature. The remaining liquid was filtered under reduced pressure using 0.45 µm nylon filter membranes to remove insoluble particles. Finally, the recovered liquid portion was diluted to (50.00 ± 0.05) ml using deionized water. For the clay, a similar procedure was used except filtration was omitted and replaced by centrifugation. Because clays tend to block filtration membranes, clay-acid mixtures were more easily separated by centrifugal force, thus enabling to recovery of the liquid part of the mixture. The conversion of the boron concentration into DOT concentration was performed by dividing the boron concentration as determined by ICP by the boron fraction (wt%), considering the stoichiometry of DOT ($Na_2B_8O_{13}.4H_2O$): [DOT] = [B] ÷ (8 M_B/M_{DOT}); where M_B = 10.811 g mol^{-1} and M_{DOT} = 412.527 g mol^{-1}. Boron standard PlasmaCal (994 ± 4) µg ml^{-1} was purchased from SCP Sciences.

Zeta Potential: The Zeta potential of clays was measured using a Zeta-Sizer Ultra (Malvern Instruments) dynamic light scattering analyzer. Sample solutions were prepared by suspending clay (40 mg), with and without DOT (0.4 and 2 mg) into deionized water (40 ml) using a rotary shaker (1 week, 40 rpm). The pH of the solutions was measured using a Mettler Toledo (ThermoFisher) pH meter with an accuracy of 0.01.

Statistical Analysis: The data were presented as the means ± standard deviation (SD) of three independent variables or more (n = 3-24) without any data transformation neither normalization process. Error bars on the graph were generated using 2SD. Outliers were identified visually on graphs and were removed from the data set when their standard deviation exceeded 30%. All results presented in tables and graphs were subjected to a single factor ANOVA test for groups larger than 3 or a *t*-test for pairing two samples for mean. P (one tail) was used in *t*-tests for the decision rule. Individual means were compared for the identification of significant differences with an α-value of 0.05. Null hypotheses were rejected when P-values were greater than α-values.

Supporting Information

Supporting Information is available from the Wiley Online Library or from the author.

Acknowledgements

This research was funded by the Pôle de Recherche et d'Innovation en Matériaux avancés du Québec (PRIMA) the Natural Sciences, Engineering Research Council of Canada (NSERC) Alliance program, Quebec Wood Export Bureau (QWEB), American Structures, Boralife Technologies Inc.. Ms. Aouinti was partly funded by the Mitacs Globalink Program. PiFM and AFM characterization was performed at NanoQAM, supported by QCAM. The authors thank Boralife Technologies Inc. for providing the treated wood.

Conflict of Interest

The authors declare no conflict of interest

Data Availability Statement

The data that support the findings of this study are available on request from the corresponding author. The data are not publicly available due to privacy or ethical restrictions.

Keywords

atomic and photoinduced force microscopy (AFM-PiFM), clay, disodium octaborate tetrahydrate (DOT), earthen construction, inductively coupled plasma optical emission spectroscopy (ICP-OES), interface, migration profile, wood

Received: May 21, 2024
Revised: July 29, 2024
Published online:

[1] T. Farid, M. I. Rafiq, A. Ali, W. Tang, *EcoMat* **2022**, *4*, e12154.
[2] E. Akpan, B. Wetzel, K. Friedrich, *Green Chem.* **2021**, *23*, 2198.
[3] M. Pramreiter, T. Nenning, L. Malzl, J. A. Konnerth, *Nat. Rev. Mat.* **2023**, *8*, 217.
[4] R. Mi, T. Li, D. Dalgo, C. Chen, Y. Kuang, S. He, X. Zhao, W. Xie, W. Gan, J. Zhu, J. Srebric, R. Yang, L. Hu, *Adv. Funct. Mater.* **2020**, *30*, 1907511.
[5] G. Wimmers, *Nat. Rev. Mat.* **2017**, *2*, 17051.
[6] P. Dabosmita, M. Gaff, D. Tesařová, D. Hui, H. Li, *Nanotech. Rev.* **2023**, *12*, 20220528.
[7] International Code Council, in *International Building Code*, Second edition, ICC Digital Codes **2021**, Ch.6: 602.3.
[8] C. Clausen, V. Yang, *Int. Biodeterior. Biodegrad.* **2007**, *59*, 2024.
[9] A. Temiz, G. Alfredsen, M. Eikenes, N. Terzıev, *Biores. Technol.* **2008**, *99*, 2102.
[10] S. Yamauchi, Y. Sakai, Y. Watanabe, M. K. Kubo, H. Matsue, *J. Wood Sci.* **2007**, *53*, 324331.
[11] P. Evans, H. Matsunaga, M. Kiguchi, *Nat. Nanotechnol.* **2008**, *3*, 577.
[12] T. Chan-Hom, W. Yamsaengsung, B. Prapagdee, T. Markpin, N. Sombatsompop, *Fire Mater.* **2017**, *41*, 675.
[13] M. Dogan, S. D. Dogan, L. A. Savas, G. Ozcelik, U. Tayfun, *Comp. Part B: Eng.* **2021**, *222*, 109088.
[14] S. Bolan, H. Wijesekara, D. Amarasiri, T. Zhang, P. Ragályi, M. Brdar-Jokanović, M. Rékási, J.-Y. Lin, L. P. Padhye, H. Zhao, L. Wang, J. Rinklebe, H. Wang, K. H. M. Siddique, M. B. Kirkham, *N. Bolan, Sci. Tot. Env.* **2023**, *894*, 1674744.
[15] M. Kabu, M. Akosman, *Rev. Env. Contam. Toxicol.* **2013**, *225*, 5775.
[16] N. Hadrup, M. Frederiksen, A. K. Sharma, *Regul. Toxicol. Pharmacol.* **2021**, *121*, 104873.
[17] S. Rompre, Boralife Technologies Inc, CA. 2 948 194, **2019**.
[18] J. B. Ra, H. M. Barnes, T. E. Conners, *Wood F. Sci.* **2001**, *33*, 90.
[19] J. E. Jakes, S. L. Zelinka, C. G. Hunt, P. Ciesielski, C. R. Frihart, D. Yelle, L. Passarini, S.-C. Gleber, D. Vine, S. Vogt, *Sci. Rep.* **2020**, *10*, 9919.
[20] C. Chen, L. Hu, *Adv. Mater.* **2020**, *33*, 2002890.
[21] J. D. Floyd, A. M. Taylor, C. Brischke, N. Irby, W. Mater, *Sci. Eng.* **2020**, *15*, 361.
[22] Y. El Meddili, M. Bouasria, M.-H. Benzaama, F. Khadraoui, M. Le Guern, D. Chateigner, S. Gascoin, J.-F. Bardeau, *Mater* **2021**, *14*, 6216.
[23] J.-C. Morel, R. Charef, E. Hamard, A. Fabbri, C. Beckett, Q.-B. Bui, *Phil. Trans. R. Soc. B* **2021**, *376*, 20200182.
[24] C. M. Ouellet-Plamondon, L. Ramseier, M. Balouktsi, L. Delem, G. Foliente, N. Francart, A. Garcia-Martinez, E. Hoxha, T. Lützkendorf, F. Nygaard Rasmussen, B. Peuportier, J. Butler, H. Birgisdottir, D. Dowdell, M. K. Dixit, V. Gomes, M. Gomes da Silva, J. C. Gómez de Cózar, M. Kjendseth Wiik, C. Llatas, R. Mateus, L. M. Pulgrossi, M. Röck, M. R. M. Saade, A. Passer, D. Satola, S. Seo, B. Soust Verdaguer, J. Veselka, M. Volf, et al., *J. Clean. Prod.* **2023**, *404*, 136834.
[25] A. Kabore, C. M. Ouellet-Plamondon, *Mater.* **2024**, *17*, 736.
[26] A. Kabore, C. M. Ouellet-Plamondon, *Ind. Crops Prod.* **2024**, *215*, 118626.
[27] A. A. Shubbar, M. Sadique, P. Kot, W. Atherton, *Constr. Build. Mat.* **2019**, *210*, 172.
[28] R. A. Schoonheydt, C. T. Johnston, F. Bergaya, in *Surface and Interface Chemistry of Clay Minerals*, Elsevier, Amsterdam **2018**.
[29] J. F. Nina, R. Eires, D. V. Oliveira, *Constr. Build. Mat.* **2023**, *3*, 143.
[30] R. Zhu, Q. Chen, Q. Zhou, Y. Xi, J. Zhu, H. He, *Appl. Clay Sci.* **2016**, *123*, 239.
[31] N. Kumari, C. Mohan, *Clay Clay Miner.* **2021**, *22*, 97672.
[32] V. Sharma, J. Yadav, R. Kumar, D. Tesarova, A. Ekielski, P. K. Mishra, *Vib. Spectrosc.* **2020**, *110*, 103097.
[33] K. E. High, K. E. H. Penkman, *Herit. Sci.* **2020**, *8*, 83.
[34] M. Vannoorenberghe, T. Van Acker, J. Belza, D. Teetaert, P. Crombé, F. Vanhaecke, *J. Anal. Atom. Spect.* **2020**, *35*, 2686.
[35] R. B. Currie, B. Kanji, A. Bruce, R. G. Schmidt, *Holzf.* **2021**, *75*, 195.
[36] Centre d'expertise en analyse environnementale du Québec, in *Détermination des métaux : méthode par spectrométrie de masse à source ionisante au plasma d'argon*, Révision 7, Ministère de l'Environnement et de la Lutte contre les changements climatiques **2020**, Ch. MA.200.
[37] W. Hyoumbi, P. Pizette, A. S. L. Wouatong, N. Abriak, *Earth Sci. Res.* **2018**, *7*, 42.
[38] M. M. Gomaa, *App. Water Sci.* **2023**, *13*, 43.
[39] E. Polidori, *Soils Found.* **2007**, *47*, 887.
[40] H. Danso, *Adv. Civ. Eng. Technol.* **2018**, *2*, 199.
[41] J.-E. Aubert, P. Faria, P. Maillard, K. Amed, J. Ouedraogo, C. Ouellet-Plamondon, E. Prud'homme, in *Testing and Characterisation of Earth-based Building Materials and Elements*, (Eds: A. Fabbri, J. C. Morel, J. E. Aubert, Q. B. Bui, D. Gallipoli, B.V. Reddy), Springer, Berlin, Germany **2021**.
[42] Standard Council of Canada, in *Soil-Determination of Liquid Limit by the Casagrande apparatus and determination of Plastic Limit*, Fifth edition, Bureau de Normalisation du Québec (BNQ) **2019**, Ch. 2501-090.
[43] F. H. Chen, in *Foundations on expansive soils*, Elsevier Science Publication, Amsterdam, **1988**.
[44] I. Yilmaz, *App. Clay Sci.* **2009**, *46*, 376.
[45] D. G. Fredlund, *Dev. Soil Sci.* **1996**, *24*, 499.
[46] V. Emmanuel, O. Barres, C. Roque, *Spectrochim. Acta A Mol. Biomol. Spectrosc.* **2015**, *136*, 1255.
[47] J. Shi, D. Xing, J. Lia, *Energy Procedia* **2012**, *16*, 758.
[48] R. M. Silverstein, F. X. Webster, D. J. Kiemle, in *Spectroscopic Identification of Organic Compounds*, John Wiley & Sons, Hoboken, NJ **2005**.
[49] G. Lefèvre, *J. Radioanal. Nucl. Chem.* **2023**, *332*, 337.
[50] J. Mao, H. Abushammala, B. Kasal, *Colloids Surf. A: Physicochem. Eng. Asp.* **2021**, *609*, 125871.
[51] A. Dazzi, C. B. Prater, *Chem. Rev.* **2017**, *117*, 5146.
[52] K. K. Kesari, P. O'Reilly, J. Seitsonen, J. Ruokolainen, T. Vuorinen, *Cellul.* **2021**, *28*, 7295.
[53] J. J. Morrell, K. M. Brooks, C. M. Davis, in *Managing Treated Wood in Aquatic Environments*, Forests Products Society, LaGrange, USA **2011**.
[54] American Society for Testing and Materials International (ASTM), *D4933-16(2021) Standard Guide for Moisture Conditioning of Wood and Wood-Based Materials*, ASTM International **2021**.
[55] E. E. Thybring, M. Fredriksson, S. L. Zelinka, S. V. Glass, *Forests* **2022**, *13*, 2051.
[56] J. Johansson, J. Salin, *Wood Mater. Sci. Eng.* **2011**, *6*, 112118.
[57] M. Borisover, J. A. Davis, *Develop. Clay Sci.* **2015**, *6*, 33.
[58] M. M. Calvino, G. Cavallaro, L. Lisuzzo, S. Milioto, G. Lazzara, *Colloids Surf. A: Physicochem. Eng. Asp.* **2022**, *641*, 128530.
[59] A. Kaya, Y. Yukselen, *Can. Geotech. J.* **2005**, *42*, 12801289.

[60] M. M. Calvino, G. Cavallaro, V. Taormina, D. Cascio, *Colloids Surf. A: Physicochem. Eng. Asp* **2019**, *576*, 22.
[61] A. Shakeel, Z. Safar, M. Ibanez, L. van Paassen, C. Chassagne, *Minerals* **2020**, *10*, 999.
[62] R. Sposito, M. Maier, N. Beuntner, K.-C. Thienel, *Constr. Build. Mater.* **2021**, *308*, 125061.
[63] T. H. Mai, T. T. K. Hong, N. T. Yen, *J. For. Sci. Technol.* **2021**, *11*, 118.